FARADAY

Calculation of cyclic voltammetric responses for the reductive formation of catalyst–substrate adducts on electrode surfaces

Yuanwu Xie, Chan Kang and Fred C. Anson*

Arthur Amos Noyes Laboratory, Division of Chemistry and Chemical Engineering, California Institute of Technology, Pasadena CA 91125, *USA*

Electrocatalysts based on monolayers of transition-metal complexes attached to electrode surfaces frequently follow mechanisms in which a chemical step is interposed between the first and subsequent electron-transfer steps. The cyclic voltammetric responses to be anticipated for such systems were calculated using finite difference procedures to solve the relevant differential equation. The calculated variation of the peak currents and peak potentials with the kinetic parameters governing the three steps in the mechanistic scheme are presented in graphical form. Application of the results to a specific experimental system, the catalysis of the electroreduction of O_2 by a macrocyclic complex of Co^{III} adsorbed on graphite electrodes, produced reasonable agreement between calculated and observed cyclic voltammograms.

The catalysis of electrode reactions that involve the transfer of multiple electrons, *e.g.* the reduction of O_2 to H_2O_2 or H_2O, may proceed by a variety of conceivable mechanisms. One way to examine possible mechanistic schemes is to compare experimental current–potential responses with those calculated on the basis of feasible mechanisms. We have employed this approach in three recent studies in which the current–potential responses to be expected were calculated for single monolayers of molecules adsorbed on electrode surfaces where they acted as catalysts in simple outer-sphere,[1] inner-sphere[2] or intramolecular[3] electron-transfer mechanisms. In the present study we extend the approach to a somewhat more complex mechanism in which a chemical reaction is interposed between the first and subsequent electron-transfer steps and a separate response appears from an intermediate in the catalytic cycle. Such ECE[4] mechanisms have been treated previously by Laviron[5,6] but only for cases where the electrode reactions were assumed to be Nernstian and the chemical reaction was assumed to be totally irreversible. We were interested in cases where these restrictive assumptions were not made, in order to compare the calculated results with those obtained in an experimental system in which the catalysed reduction of O_2 to H_2O_2 by a complex of Co^{III} adsorbed on the surface of graphite electrodes appeared to proceed by such an ECE mechanism.[7] In our previous reports[1–3] the calculational procedures employed were based primarily on the original treatments of Andrieux and Saveant[8] and Aoki *et al.*[9] as elaborated and extended to encompass the mechanistic schemes of interest. In the present case it was possible to carry out all of the necessary calculations using finite difference procedures.[10] Because of the availability of previous descriptions of the details of the calculations they are only outlined in the present report.

The mechanism we wish to consider is depicted in Scheme I:

$$(O)_{ads} + e \rightleftharpoons (R)_{ads}; \qquad E_1^f, k_{s_1}^0, \alpha_1 \qquad (1)$$

$$(R)_{ads} + Z \underset{k_{-2}}{\overset{k_2}{\rightleftharpoons}} (R{-}Z)_{ads}; \qquad k_2, k_{-2}, K_2 \qquad (2)$$

$$(R{-}Z)_{ads} + e \rightleftharpoons (R{-}Z^{\cdot})_{ads} \qquad E_3^f, k_{s_3}^0, \alpha_3 \qquad (3)$$

The catalyst, consisting of the O/R couple, is confined in a monolayer on the electrode surface. The substrate, Z, can be reduced only after it is bound by the reduced form of the catalyst to form the adduct, $(R{-}Z)_{ads}$. This reaction is governed by equilibrium and rate constants, K_2, k_2 and k_{-2}. The adduct, $(R{-}Z)_{ads}$, is reduced in half-reaction (3) which is characterized by the formal potential E_3^f, standard rate constant $k_{s_3}^0$ and transfer coefficient α_3. If the reduced adduct, $(R{-}Z^{\cdot})_{ads}$, is stable, the reduction of Z ceases as soon as all of the O/R catalyst present on the electrode surface is converted to $(R{-}Z^{\cdot})_{ads}$. In cases where $(R{-}Z^{\cdot})_{ads}$ can be further reduced to produce an unbound product with the reformation of $(R)_{ads}$, a catalytic reduction of Z ensues. The combination where R is a macrocyclic complex of cobalt(II) and Z is O_2 represents one specific example of such a catalytic system[7] to which we will return. However, the voltammetric responses to be expected from systems which adhere to the simpler, non-catalytic mechanism given in Scheme I will be considered first.

The calculations were carried out using the following assumptions or conditions: The quantity of the O/R catalyst present on the electrode surface, Γ, was assumed to remain unchanged:

$$\Gamma = \Gamma_O + \Gamma_R + \Gamma_{R-Z} + \Gamma_{R-Z^{\cdot}} \qquad (I)$$

For cases where the two electrode reactions adhere to the Nernst equation one has

$$\frac{\Gamma_O}{\Gamma_R} = \exp\left[\frac{F}{RT}(E - E_1^f)\right] = \theta_1 \qquad (II)$$

and

$$\frac{\Gamma_{R-Z}}{\Gamma_{R-Z^{\cdot}}} = \exp\left[\frac{F}{RT}(E - E_3^f)\right] = \theta_3 \qquad (III)$$

For cases where the electrode reactions are not Nernstein, the concentrations of the reactants present on the electrode surface are calculated from eqn. (IV) and (V)

$$\frac{d\Gamma_O}{dt} = -k_{s_1}^0\left\{\Gamma_O \exp\left[\frac{-\alpha_1 F}{RT}(E - E_1^f)\right] - \Gamma_R \exp\left[\frac{(1-\alpha_1)F}{RT}(E - E_1^f)\right]\right\} \qquad (IV)$$

$$\frac{d\Gamma_{R-Z}}{dt} = k_{s_3}^0\left\{\Gamma_{R-Z} \exp\left[\frac{-\alpha_3 F}{RT}(E - E_3^f)\right] - \Gamma_{R-Z^{\cdot}} \exp\left[\frac{(1-\alpha_3)F}{RT}(E - E_3^f)\right]\right\} \qquad (V)$$

For cases where reaction (2) remains at equilibrium

$$\frac{\Gamma_{R-Z}}{\Gamma_R} = K_2 C_Z(0, t) \quad \text{(VI)}$$

where $C_Z(0, t)$ is the concentration of Z at the electrode surface. If reaction (2) does not remain at equilibrium, eqn. (VII) is used in place of eqn. (VI)

$$k_2 C_Z(0, t)\Gamma_R - k_{-2}\Gamma_{R-Z} = -\frac{d(\Gamma_O + \Gamma_R)}{dt} = \frac{d(\Gamma_{R-Z} + \Gamma_{R-Z'})}{dt} \quad \text{(VII)}$$

As the consumption of Z at the electrode surface is limited by the quantity of $(R)_{ads}$ present on the electrode surface, the value of $C_Z(0, t)$ may remain essentially constant if the concentration of Z in the bulk of the solution, C_Z^0, is large enough. For cases where $C_Z(0, t)$ does not remain constant, its value can be calculated using finite difference methods[10] as applied to eqn. (VIII) and (IX)

$$\frac{\partial C_Z(x, t)}{\partial t} = -\frac{\partial J_Z(x, t)}{\partial x} \quad \text{(VIII)}$$

where $J_Z(x, t)$ is the flux of Z and, at the electrode surface,

$$J_Z(0, t) = -D_Z\left[\frac{\partial C_Z(x, t)}{\partial x}\right]_{x=0} + \frac{d[\Gamma_{R-Z} + \Gamma_{R-Z'}]}{dt} \quad \text{(IX)}$$

where D_Z is the diffusion coefficient of Z.

The total observed current, I_t, will be the sum of the contributions from half-reactions (1) and (3)

$$I_1 = FS\left(-\frac{d\Gamma_O}{dt}\right) \quad \text{(X)}$$

$$I_3 = FS\left(\frac{d\Gamma_{R-Z'}}{dt}\right) \quad \text{(XI)}$$

$$I_t = I_1 + I_3 \quad \text{(XII)}$$

or, in dimensionless form,

$$\psi_1 = I_1\left[\frac{F^2}{RT} Sv\Gamma\right]^{-1} \quad \text{(XIII)}$$

$$\psi_3 = I_3\left[\frac{F^2}{RT} Sv\Gamma\right]^{-1} \quad \text{(XIV)}$$

$$\psi_t = \psi_1 + \psi_3 \quad \text{(XV)}$$

where S is the electrode area and v is the rate at which the electrode potential is scanned from its initial value, E_i

$$E = E_i - vt \quad \text{(XVI)}$$

Results and Discussion

It will be convenient to divide the analysis into two broad categories: Situations in which $C_Z(0, t)$ can be assumed to remain constant at C_Z^0 comprise the first category. The second involves situations where $C_Z(0, t)$ changes as the voltammogram is recorded. Within each category several cases will be examined. The cases are differentiated on the basis of the rates of reactions (1)–(3).

Category I; $C_Z(0, t) = C_Z^0$

Case (i). Half-reactions (1) and (3) are Nernstian; reaction (2) remains at equilibrium ($k_{s_1}^0, k_{s_3}^0, k_2, k_{-2} \rightarrow \infty$).

The combination of eqn (I)–(III), (VI) and (XVI) leads to expressions for Γ and $\Gamma_{R-Z'}$ whose time derivatives [using $(d\Gamma_i/dt) = -v(d\Gamma_i/dE)$] give eqn. (XVII) and (XVIII)

$$-\frac{d\Gamma_O}{dt} = \frac{vFT}{RT}\theta_1\theta_3 \times \frac{[2K_2 C_Z^0 + (1 + K_2 C_Z^0)\theta_3]}{[K_2 C_Z^0 + (1 + K_2 C_Z^0)\theta_3 + \theta_1\theta_3]^2} \quad \text{(XVII)}$$

$$\frac{d\Gamma_{R-Z'}}{dt} = \frac{vFT}{RT} K_2 C_Z^0 \times \frac{[(1 + K_2 C_Z^0)\theta_3 + 2\theta_1\theta_3]}{[K_2 C_Z^0 + (1 + K_2 C_Z^0)\theta_3 + \theta_1\theta_3]^2} \quad \text{(XVIII)}$$

The dimensionless current–potential curves can then be calculated directly from eqn. (X)–(XV). The results of such calculations are shown in Fig. 1 for various values of $K_2 C_Z^0$ and $(E_3^f - E_1^f)$. In Fig. 1A the formal potentials of half-reactions (1) and (3) are assumed to be equal and the value of $K_2 C_Z^0$ is varied between 10^{-3} and 10^3 corresponding, respectively, to little or extensive equilibrium formation of the reducible adduct $(R{-}Z)_{ads}$. Because the two electrode reactions are taken to be Nernstian, the cathodic and anodic peak potentials are identical. When $K_2 C_Z^0$ is much less than unity (curves a and b in Fig. 1A) two separated current peaks appear in the voltammogram despite the fact that E_1^f and E_3^f were taken as equal. The first peak appears near E_1^f but the second appears at potentials notably more negative than E_3^f. The two peaks move together as $K_2 C_Z^0$ is increased and merge into a single larger peak when $K_2 C_Z^0$ is unity (curve d in Fig. 1A). At larger values of $K_2 C_Z^0$, separate, smaller peaks develop again with one centred near E_3^f $(= E_1^f)$ and the other at much more positive potentials (curves f and g in Fig. 1A). When well separated peaks are obtained, the width at half-height of each is $3.53RT/F = 90.4$ mV and the dimensionless peak current of each is 0.25.

In Fig. 1B–D are shown the responses calculated for cases where E_1^f and E_3^f are unequal and $K_2 C_Z^0$ is 10^{-2}, 1 or 10^2. When E_3^f is much more negative than E_1^f and $K_2 C_Z^0$ is small (10^{-2}) the response contains two separated peaks (curves a and b in Fig. 1B). The separation between the two peaks diminishes as E_3^f approaches E_1^f (curves c, d) and when E_3^f is much more positive than E_1^f, a single peak results at a potential between E_1^f and E_3^f and with a dimensionless peak current of 1.0 (curve h in Fig. 1B). The width of curve h is $1.76RT/F = 45.1$ mV and it has all the characteristics of a single, two-electron reaction. The behaviour is qualitatively similar with larger values of $K_2 C_Z^0$ (Fig. 1C and D).

Under circumstances where two peaks are present in the voltammogram and K_2 is known, the value of E_3^f may be calculated from the combination of eqn. (XIX) and (XX)

$$\theta_1' = 1 + K_2 C_Z^0 + \frac{K_2 C_Z^0}{\theta_3'} - \frac{2K_2 C_Z^0(1 + K_2 C_Z^0)}{(1 + K_2 C_Z^0)\theta_3' + 4K_2 C_Z^0} \quad \text{(XIX)}$$

$$\theta_3'' = \frac{K_2 C_Z^0(1 + K_2 C_Z^0) + 4K_2 C_Z^0 \theta_1''}{(1 + K_2 C_Z^0)^2 + 3(1 + K_2 C_Z^0)\theta_1'' + 4(\theta_1'')^2} \quad \text{(XX)}$$

where

$$\theta_1' = \exp\left[\frac{F}{RT}(E_{p1} - E_1^f)\right] \quad \text{(XXI)}$$

$$\theta_3' = \exp\left[\frac{F}{RT}(E_{p1} - E_3^f)\right] \quad \text{(XXII)}$$

$$\theta_1'' = \exp\left[\frac{F}{RT}(E_{p2} - E_1^f)\right] \quad \text{(XXIII)}$$

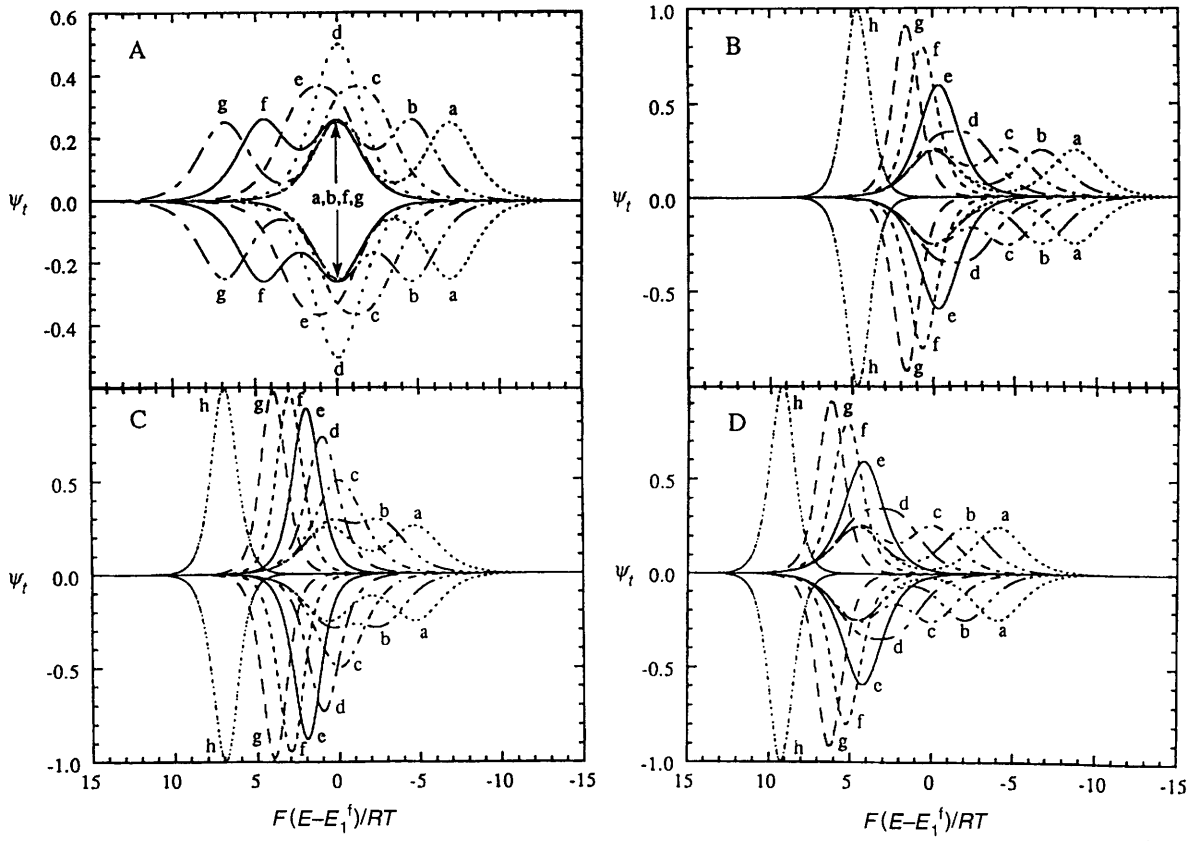

Fig. 1 Cyclic voltammetric responses calculated for case (i) of Scheme I (see text) with $C_Z(0, t) = C_Z^0$. A, $E_3^f = E_1^f$; $K_2 C_Z^0$ = a, 10^{-3}; b, 10^{-2}; c, 10^{-1}; d, 1; e. 10; f, 10^2; g, 10^3. B–D, $F/RT(E_3^f - E_1^f)$ = a, −4; b, −2; c, 0; d, 2; e, 4; f, 6; g, 8; h, 14 and $K_2 C_Z^0$ = B, 10^{-2}; C, 1, D, 10^2.

$$\theta_3'' = \exp\left[\frac{F}{RT}(E_{p2} - E_3^f)\right] \qquad \text{(XXIV)}$$

and E_{p1} and E_{p2} are the two observed peak potentials (cathodic or anodic since they are the same). Eqn. (XIX) and (XX) were obtained by setting the derivatives of the right-hand sides of eqn. (XVII) and (XVIII) equal to zero at the two peak potentials.

In cases where C_Z^0 cannot be increased or decreased sufficiently to cause two peaks to appear in the voltammogram, E_3^f may still be estimated if it is much more positive than E_1^f and $K_2 C_Z^0$ is not extremely small or large. Under these conditions, and if the peak potential of the single observed peak, E_p^*, satisfies the condition $E_1^f \ll E_p^* \ll E_3^f$, it follows that $\theta_3' \ll 1$, eqn. (XIX) simplies to $\theta_1' \sim K_2 C_Z^0/\theta_3'$ and leads to eqn. (XXV)

$$E_p^* = 0.5(E_1^f + E_3^f) + \frac{RT}{2F}\ln(K_2 C_Z^0) \qquad \text{(XXV)}$$

Thus, E_3^f can be calculated from the observed value of E_p^* if K_2 is known.

Case (ii). Half-reactions (1) and (3) are Nernstian; reaction (2) is not at equilibrium ($k_{s1}^0, k_{s3}^0 \to \infty$; $k_2, k_{-2} < \infty$).

When the formation of $(R{-}Z)_{ads}$ is not instantaneous, the voltammetric responses are calculated from eqn. (I)–(III) and (VII). It is convenient to characterize the kinetics of reaction (2) by a dimensionless kinetic parameter, r_2,

$$r_2 \equiv \frac{k_2 C_Z^0 RT}{vF} \qquad \text{(XXVI)}$$

Shown in Fig. 2A is a set of voltammetric responses for various values of r_2 and fixed values of K_2, and $E_3^f - E_1^f$. When r_2 is sufficiently large, case (ii) becomes case (i) and symmetrical responses like that in curve a of Fig. 2A are obtained with identical cathodic and anodic peak potentials. As r_2 decreases, the cathodic peak current diminishes and the peak potential shifts toward E_1^f while the anodic peak diminishes and shifts towards E_3^f as shown in curves b–g in Fig. 2A. The increase in the dimensionless peak currents as the scan rate decreases means that the actual peak currents are not proportional to the scan rate, which is a diagnostically useful property (*vide infra*). For some combinations of r_2 and the range

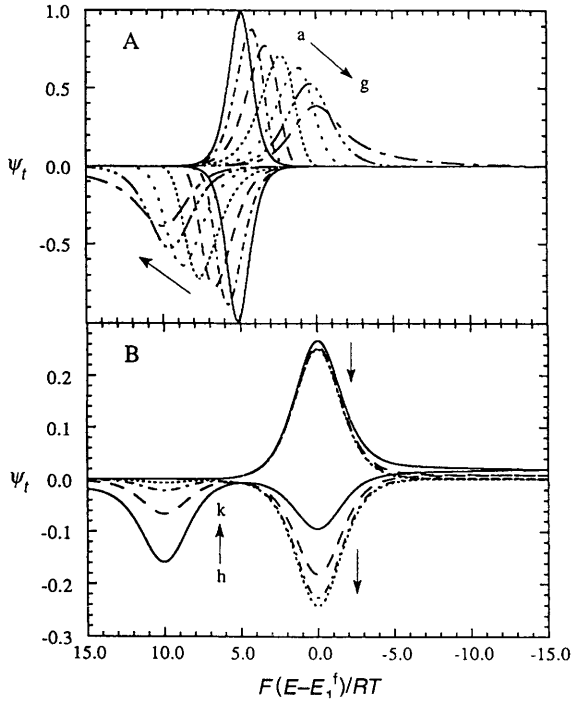

Fig. 2 Cyclic voltammetric responses calculated for case (ii) of Scheme I (see text) with $C_Z(0. t) = C_Z^0$, $K_2 C_Z^0 = 1$ and $F/RT(E_3^f - E_1^f) = 10$. A, r_2 = a, 10^3; b, 10^2; c, 30; d, 10; e, 3; f, 1; g, 0.3. B, as in A with an expanded (dimensionless) current scale and r_2 = h, 3×10^{-2}; i, 10^{-2}; j, 3×10^{-3}; k, 10^{-3}.

over which the potential is scanned, a pair of responses can be obtained with matching anodic and cathodic peak potentials as shown in Fig. 2B. If this circumstance can be realized, the value of E^f_3 can be read directly from the position of the single anodic peak. In cases where a response like those in Fig. 2B cannot be obtained (because impractical scan rates would be necessary) it is still possible to obtain estimates of E'_3 from the anodic and cathodic peak potentials of responses like those shown in Fig. 2A. By carrying out calculations for a variety of conditions we observed that both peak potentials are linearly related to $\ln(r_2)$ (*i.e.* ln *v*) over a reasonable range of scan rates. This linearity is demonstrated in the plots shown in Fig. 3A. The peak potentials were taken from calculated responses like those in Fig. 2A. The range of linearity of plots like those in Fig. 3A depends upon the difference between E^f_1 and E^f_3 as is shown in Fig. 3B. The intersections of the two linear plots of the anodic and cathodic peak potentials *vs.* ln r_2 occur at E^*_p [Eqn. (XXV)] so that plots like those in Fig. 3A and 3B can be used to evaluate E^*_p, the common anodic and cathodic peak potential that would be observed if reaction (2) remained at equilibrium. The intersection point occurs at larger values of r_2 as $F/RT(E^f_3 - E^f_1)$ becomes more positive (Fig. 3B) which reflects the fact that larger values of k_2 and k_{-2} are required to keep reaction (2) at equilibrium as E^f_3 becomes more positive. The reason is that less and less $(R{-}Z)_{ads}$ is present on the electrode as E^*_p becomes more positive (because E^f_3 is more positive) so that larger rate constants are needed to compensate for the smaller effective concentration of the reactant participating in reaction (2).

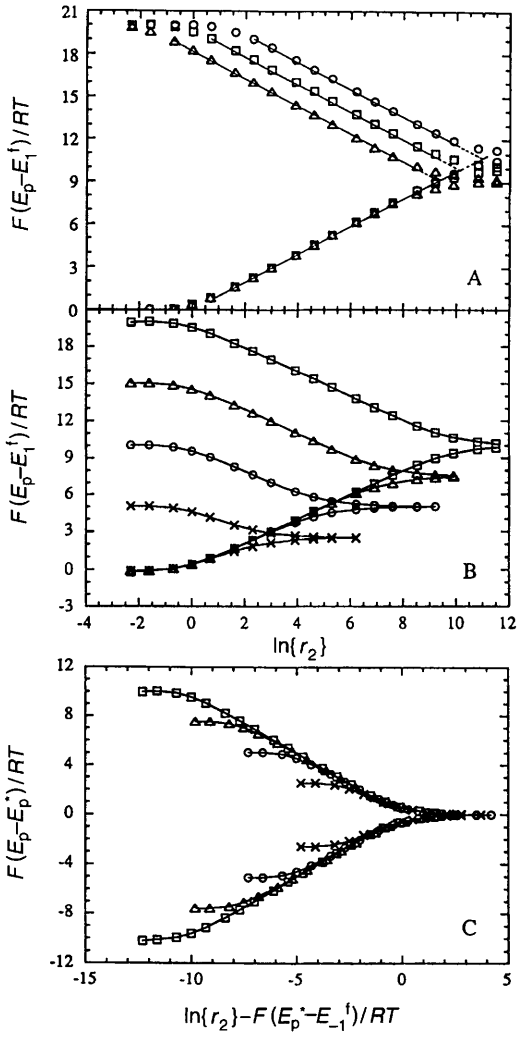

Fig. 3 Anodic and cathodic peak potentials, E_p, *vs.* the kinetic parameter for case (ii). A, B, anodic (upper lines) and cathodic (lower line) peak potentials *vs.* ln r_2 with A, $F/RT(E^f_3 - E^f_1) = 20$ and $K_2C^0_Z = (\triangle)$ 0.2, (○) 1, (□) 5 or B, $K_2C^0_Z = 1$ and $F/RT(E^f_3 - E^f_1) =$ (□) 20, (△) 15, (○) 10, (×) 5. C, composite plot of the data in A and B from which r_2 may be estimated as described in the text.

The behaviour shown in Fig. 3A and B can be exhibited in the more 'universal' format shown in Fig. 3C which provides a means for estimating r_2 (*i.e.* k_2). Once E^*_p is obtained from the intersections of plots like those in Fig. 3A or B, the corresponding value of $(E_p - E^*_p)$ at any scan rate leads, *via* Fig. 3C, to a value of $\ln r_2 - F/RT(E^*_p - E^f_1)$ in which the only unknown is r_2 so that k_2 can be calculated. In carrying out this analysis, scan rates that correspond to the inclined portions of the curves in Fig. 3C would need to be employed to obtain the most reliable estimates of r_2.

Case (iii). Half-reaction (1) is Nernstian, half-reaction (3) is not; reaction (2) is at equilibrium ($k^0_{s_1}, k_2, k_{-2} \rightarrow \infty$; $k^0_{s_3} < \infty$.

When the second electron-transfer step is slow, the voltammetric responses to be expected can be calculated from Eqn. (I), (II), (V) and (VI). It is convenient to introduce a dimensionless parameter to characterize the kinetics of half-reaction (3)

$$m_3 = \frac{k^0_{s_3} RT}{vF} \qquad \text{(XXVII)}$$

Calculated voltammetric responses are shown in Fig. 4A for various values of m_3 with E^f_3 taken to be much more positive than E^f_1. A notable feature is the nearly constant dimensionless anodic peak current when the separation between anodic and cathodic peaks reaches *ca.* $5F/RT$. Under these conditions the actual anodic peak currents increase linearly with the scan rate, a property which allows discrimination between cases (ii) and (iii).

When m_3 is large, the anodic and cathodic peak potentials are close together (curve h in Fig. 4A). As m_3 decreases the anodic and cathodic peaks shift apart, the anodic peak shifting more rapidly than the cathodic peak (Fig. 4A). Plots of the two peak potentials *vs.* ln m_3 for several values of the transfer coefficient for half-reaction (3) are shown in Fig. 4B. The plots are linear over a reasonable range of m_3 (*i.e.* scan rates) and the intersections of the extrapolated lines all occur at the same potential which turns out to be *ca.* 15 mV more negative than E^*_p for any combination of the values of $K_2C^0_Z$, α_3 and E^f_3. Thus, the intersection point provides a rough estimate of E^f_3.

The slopes of the lines of Fig. 4B are quite different for the anodic and cathodic peak potentials. This behaviour differs from that in the corresponding plots for case (ii) (Fig. 3A) and provides another means for distinguishing between cases (ii) and (iii).

Shown in Fig. 4C is a 'universal' plot which may be used to estimate $k^0_{s_3}$ and α_3 from the anodic peak potentials, E_{pa}, measured at various scan rates (*i.e.* values of m_3). As long as $F/RT(E^f_3 - E^f_1)$ is large enough, a single line is obtained for various values of $K_2C^0_Z$ and α_3. Approximate values of $F/RT(E_{pa} - E^f_3)$ are accessible at various scan rates from the measured values of E_{pa} and the intersection potential of plots like those in Fig. 4B. The corresponding values of $\ln m_3 - \alpha_3 F/RT(E_{pa} - E^f_3)$ read from the line in Fig. 4C can then be used to calculate both α_3 and $k^0_{s_3}$ (from m_3).

For smaller values of $F/RT(E^f_3 - E^f_1)$, deviations from linearity develop in the plot of Fig. 4C as m_3 increases. A few examples are shown in Fig. 4D.

Case (iv). Half-reaction (1) is Nernstian; half-reaction (3) is not; reaction (2) is not at equilibrium ($k^0_{s_1} \rightarrow \infty$; $k^0_{s_3} k_2, k_{-2} < \infty$).

For this case the voltammetric responses are influenced by both of the previously defined kinetic parameters, r_2 and m_3. Calculations were carried out using eqn. (I) (II), (V) and (VII) and some of the results are compared with those for cases (ii) and (iii) in Fig. 5A. Curve a corresponds to case (iii) with $r_2 \rightarrow \infty$ and $m_3 = 1$ while curve b corresponds to case (ii) with

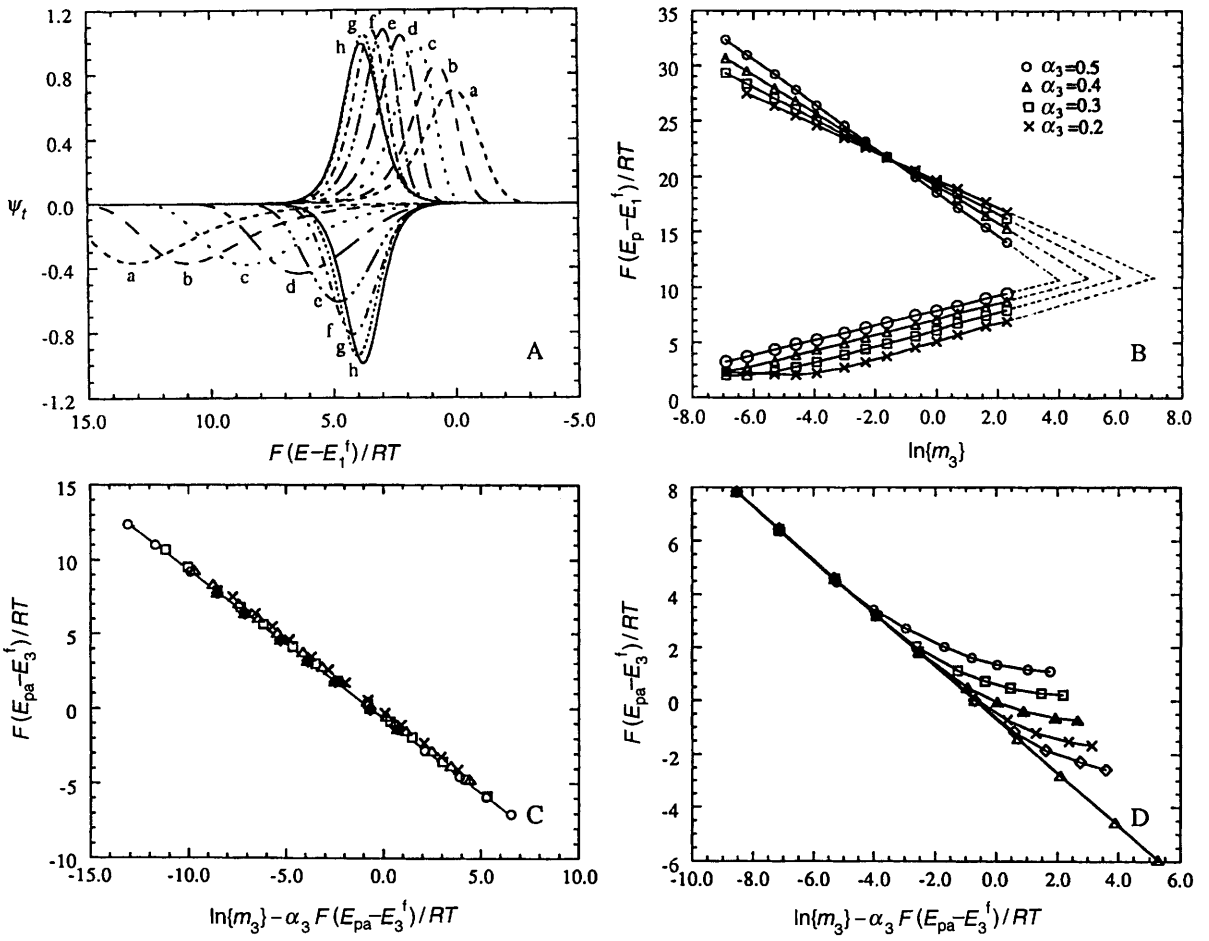

Fig. 4 A, Cyclic voltammetric responses calculated for case (iii) of Scheme I (see text) with $C_Z(0, t) = C_Z^0$, $K_2 C_Z^0 = 0.1$, $F/RT(E_3^f - E_1^f) = 10$ and m_3 = a, 0.1; b, 0.3; c, 1; d, 3; e, 10; f, 30; g, 10^2; h, ∞. B, Anodic (upper lines) and cathodic (lower lines) peak potentials *vs.* ln m_3 for $K_2 C_Z^0 = 10$, $F/RT(E_3^f - E_1^f) = 20$ and various values of α_3. C, D, Composite plots of anodic peak potentials (for $K_2 C_Z^0 = 10$) from which values of m_3 may be estimated (see text). C, (○) $K_2 C_Z^0 = 10$, $\alpha_3 = 0.5$, $E_3^f = E_1^f + 20(RT/F)$; (□) $K_2 C_Z^0 = 10$, $\alpha_3 = 0.4$, $E_3^f = E_1^f + 20(RT/F)$; (△) $K_2 C_Z^0 = 10$, $\alpha_3 = 0.3$, $E_3^f = E_1^f + 20(RT/F)$; (×) $K_2 C_Z^0 = 10$, $\alpha_3 = 0.2$, $E_3^f = E_1^f + 20(RT/F)$; (◇) $K_2 C_Z^0 = 100$, $\alpha_3 = 0.5$, $E_3^f = E_1^f + 10(RT/F)$; (▲) $K_2 C_Z^0 = 1.0$, $\alpha_3 = 0.5$, $E_3^f = E_1^f + 14(RT/F)$. D, $E_3^f = $ (○) E_1^f, (□) $E_1^f + 2.0(RT/F)$, (▲) $E_1^f + 4.0(RT/F)$, (×) $E_1^f + 6.0(RT/F)$, (◇) $E_1^f + 8.0(RT/F)$, (△) $E_1^f + 20.0(RT/F)$.

$r_2 = 1$ and $m_3 \rightarrow \infty$. The separation between the anodic and cathodic peak potentials is greater for curve a than for curve b because the rate of half-reaction (3), but not of reaction (2), is influenced by changes in the electrode potential. Curve d was calculated for case (iv) with $r_2 = m_3 = 1$. The cathodic peak is almost identical to that for case (ii) which means that the cathodic current is controlled primarily by the kinetics of reaction (2) even though $r_2 = m_3$. The anodic peak current for curve d is smaller and the peak potential more positive than those for curve a or curve b which indicates that the kinetics of both reaction (2) and half-reaction (3) affect the anodic response. Curve c, which resulted when m_3 was increased to 10 with $r_2 = 1$, essentially coincides with curve b, as expected for control of the response by the kinetics of reaction (2). Curve e resulted from the converse combination of kinetic parameters ($r_2 = 10$, $m_3 = 1$). The separation between the peak potentials is smaller than that for curve c, as expected for the higher value of k_2 corresponding to the larger value of r_2.

The linear plots obtained if the anodic and cathodic peak potentials are plotted *vs.* ln v are shown in Fig. 5B. Their slopes depend upon the two kinetic parameters but their intersection points provide approximate values for E_p^* from which E_3^f may be estimated from eqn. (XXV) if K_2 is known.

Category II: $C_Z(0, t)$ is time dependent

When it is not convenient or possible to employ substrate concentrations high enough to prevent its depletion at the electrode surface, the effects of the diffusion of Z to the electrode surface have to be taken into account by means of finite difference calculations using eqn. (VIII) and (IX). The results of some selected calculations for cases (i), (ii) and (iii) are summarized in Fig. 6. In Fig. 6A are shown voltammograms calculated for case (i) where the small changes in the peak positions and shapes are caused by changes in the total quantity of catalyst present on the electrode surface. The outermost dotted curve corresponds to curve d in Fig. 1A where $C_Z(0, t)$ is constant.

The responses expected for case (ii) are shown in Fig. 6B. The dotted curves are for constant $C_Z(0, t)$ and the solid curves are those calculated when $C_Z(0, t)$ changes. As C_Z^0 is decreased (curves a–e), the cathodic peak currents decrease because of the diminished rate at which $(R{-}Z)_{ads}$ is formed. However, the anodic peak current remains unchanged as long as the conditions (scan rate, range of the potential scan, value of r_2) are such that all of the catalyst on the electrode surface is converted to $(R{-}Z^{\cdot})$ by the time the potential reaches the range where the anodic oxidation begins. At the lowest values of C_Z^0 the cathodic response develops a diffusive 'tail' (curves d and e) because longer times are required for sufficient Z to diffuse to the electrode surface to react with all of the $(R)_{ads}$ generated there.

For case (iii) (Fig. 6C) the cathodic peaks are not as sensitive to changes in C_Z^0 as for case (ii). The anodic peak is broadened and diminished by the finite rate of half-reaction (3) but it is not dependent on C_Z^0 under conditions where the same quantity of $(R{-}Z^{\cdot})_{ads}$ is generated on the electrode surface during each reductive half-cycle.

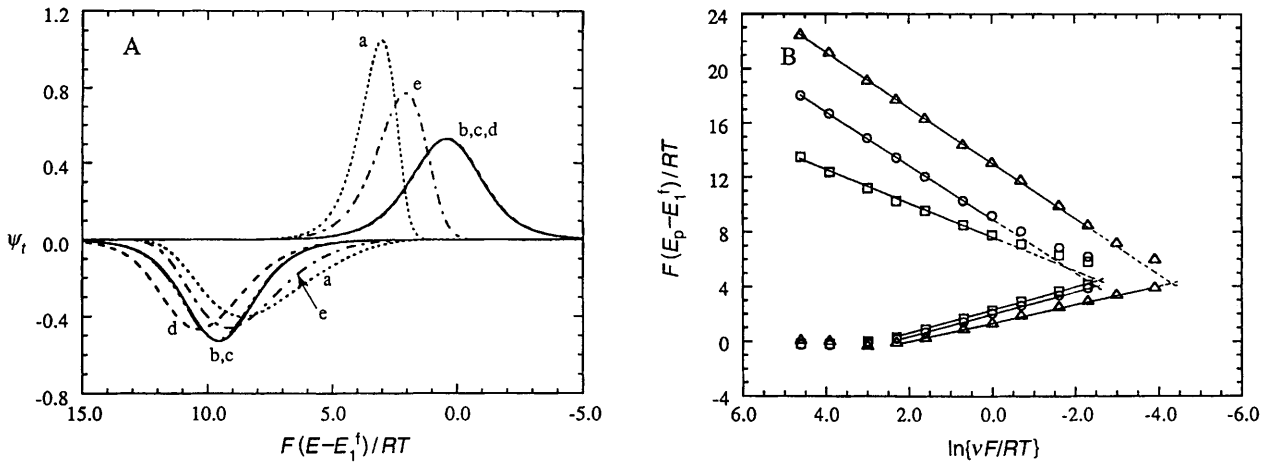

Fig. 5 A, Cyclic voltammetric responses calculated for case (iv) of Scheme I (see text) with $C_Z(0, t) = C_Z^0$, $K_2 C_Z^0 = 0.1$, $F/RT(E_3^f - E_1^f) = 10$, $\alpha_3 = 0.5$ and m_3, r_2 = a, 1, ∞; b, ∞, 1; c, 10, 1; d, 1, 1; e, 1, 10. B, Anodic (upper lines) and cathodic (lower lines) peak potentials *vs.* scan rate for the parameters in A except $K_2 C_Z^0$, $k_{s_3}^0(s^{-1})$ = (△) 10^2, 1; (○) 10, 10; (□) 10, 1.

It proved possible to characterize the behaviour of a variety of systems from both category I and category II in terms of a single dimensionless parameter, Y, defined in eqn. (XXVIII)

$$Y \equiv \frac{C_Z^0}{\Gamma}\left(\frac{RTD_Z}{Fv}\right)^{1/2} \qquad \text{(XXVIII)}$$

Plotted in Fig. 6D are 'universal' curves giving the calculated values of the dimensionless cathodic peak current as a function of ln Y for cases (i), (ii) and (iii). The peak current is quite sensitive to the experimental parameters between ln $Y = -2$ and ln $Y = +2$. When ln Y is smaller than *ca.* -2 the dimensionless peak current remains close to 0.25 and there is essentially no contribution to the current from half reaction (3). For values of ln Y greater than *ca.* 2, $C_Z(0, t)$ remains essentially constant and the analyses presented for category I apply.

Application to a specific system

An experimental example of a system that adheres to the reaction mechanism depicted in Scheme I is provided by the complex of cobalt(III) with the macrocyclic ligand hmc

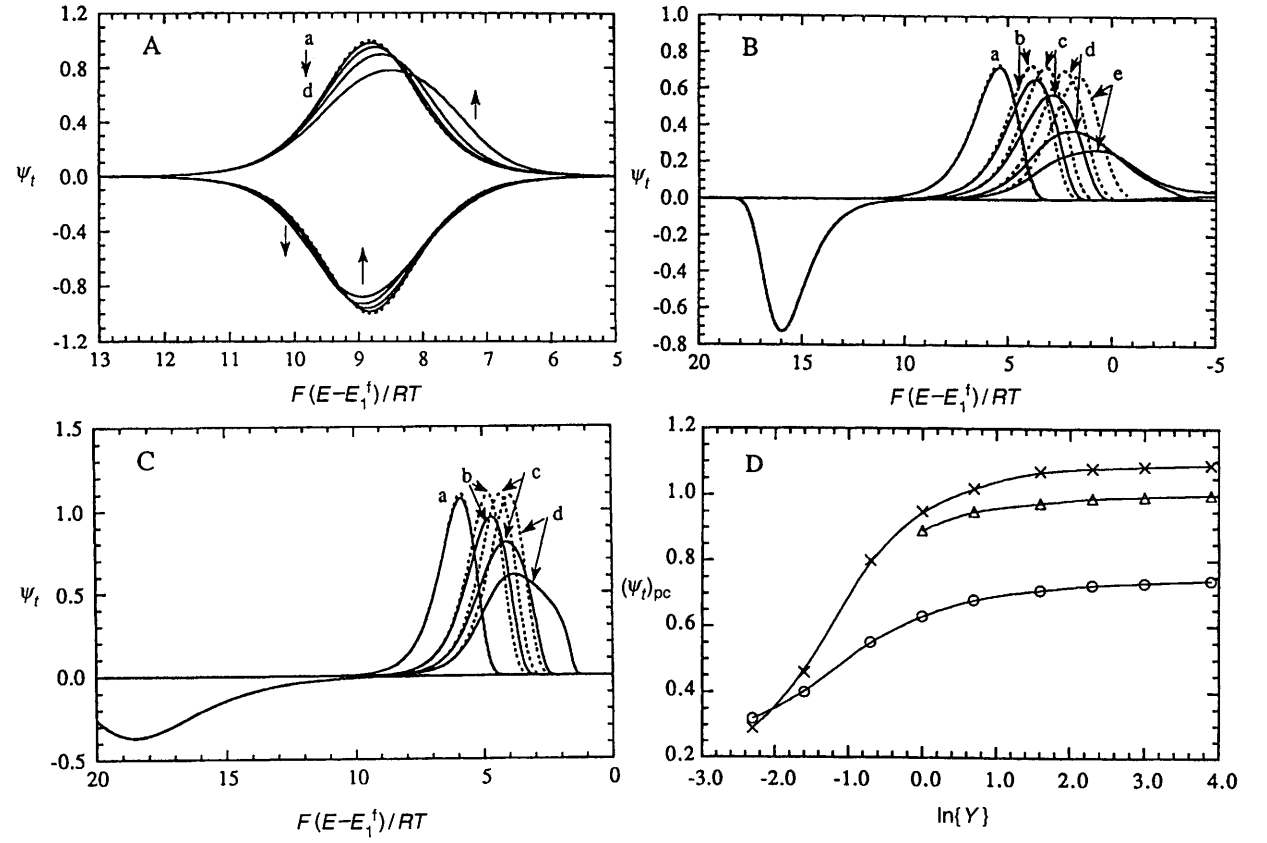

Fig. 6 Cyclic voltammetric responses calculated for Scheme I under conditions where $C_Z(0, t)$ is not constant. $F/RT(E_3^f - E_1^f) = 20$, $K_2 = 10^3$ M^{-1}, $D_Z = 4 \times 10^{-6}$ cm^2 s^{-1}, $vF/RT = 1$ s^{-1} and A, case (i) with $C_Z^0 = 10^{-4}$ M and Γ(mol cm^{-2}) = a, 10^{-11}; b, 4×10^{-11}; c, 10^{-10}; d, 2×10^{-10}. B, Case (ii) with $\Gamma = 2 \times 10^{-10}$ mol cm^{-2} and $k_2 = 5 \times 10^5$ M^{-1} s^{-1} and C_Z^0 (M) = a, 10^{-5}; b, 2×10^{-5}; c, 5×10^{-5}; d, 10^{-4}; e, 5×10^{-4}. C, Case (iii) with $\Gamma = 2 \times 10^{-10}$ mol cm^{-2}, $k_{s_3}^0 = 1$ s^{-1}, $\alpha_3 = 0.5$ and C_Z^0(M) = a, 5×10^{-4}; b, 10^{-4}; c, 5×10^{-5}; d, 1.3×10^{-5}. In every case the dotted curves correspond to $C_Z(0, t) = C_Z^0$. D, Dependence of dimensionless cathodic peak currents on a composite parameter (see text) with $F/RT(E_3^f - E_1^f) = 20$ and (△) case (i), $K_2 C_Z^0 = 0.1$, (○) case (ii), $k_2 = 10^5$ M^{-1} s^{-1}, $K_2 = 10^3$ M^{-1}, $C_Z^0 = 10^{-4}$ M, (×) case (iii), $k_{s_3}^0 = 0.1$ s^{-1} $K_2 C_Z^0 = 0.1$.

(hmc = *C-meso*-5,7,7,12,14,14-hexamethyl-1,4,8,11-tetraazacyclotetradecane) irreversibly adsorbed on the surface of a graphite electrode where it catalyses the reduction of O_2.[7] The first three steps in the catalytic mechanism are shown in reactions (4)–(6).

$$[(hmc)Co]_{ads}^{3+} \rightleftharpoons [(hmc)Co]_{ads}^{2+}; \quad E_1^f, k_{s_1}^0, \alpha_1 \quad (4)$$

$$[(hmc)Co]_{ads}^{2+} + O_2 \rightleftharpoons [(hmc)CoO_2]_{ads}^{2+}; \quad k_2, k_{-2}, K_2 \quad (5)$$

$$[(hmc)CoO_2]_{ads}^{2+} + e + H^+ \rightleftharpoons [(hmc)CoO_2H]_{ads}^{2+}; \quad E_3^f, k_{s_3}^0, \alpha_3 \quad (6)$$

The values of α_1, $k_{s_1}^0$, E_1^f and K_2 were available from a previous study.[7] A value of 0.66 V was estimated for E_3^f from the intersection of the plots shown in Fig. 7A using Eqn. (XXV). Estimates of k_2, α_3 and $k_{s_3}^0$ were obtained by fitting calculated current–potential curves to the experimental curves. For example, the dotted line in Fig. 7B was calculated to fit the experimental currents shown by the open circles. The agreement between the calculated and experimental currents is reasonably good except at the point where the scan direction is reversed and at the anodic peak. The better agreement shown by the solid line in Fig. 7B resulted when account was taken of the further reduction of the $[(hmc)CoO_2H]_{ads}^{2+}$ complex [half-reaction (7)].

$$[(hmc)CoO_2H]_{ads}^{2+} + e + H^+ \rightarrow [(hmc)Co]_{ads}^{2+} + H_2O_2; \quad E_4^f, \alpha_4, k_{s_4}^0 \quad (7)$$

The peak current for the reduction of $[(hmc)CoO_2H]_{ads}^{2+}$ occurs at a considerably less positive potential (0.06 V, ref. 7) than the cathodic peak in Fig. 7B, but sufficient reduction proceeds during the recording of the cathodic peak in Fig. 7B to diminish slightly the quantity of $[(hmc)CoO_2H]_{ads}^{2+}$ that controls the magnitude of the anodic current in Fig. 7B. When this small correction was included in the calculations the solid curve in Fig. 7B was obtained. The experimental conditions corresponded to case (ii) of category II with $F/RT(E_3^f - E_1^f) > 20$. The comparison of the calculated and observed responses in Fig. 7B provided a reasonable basis for assigning the mechanism depicted in reactions (4)–(6) to the $(hmc)Co^{3+/2+}$–O_2 system with the kinetic parameters indicated in the caption of Fig. 7B.

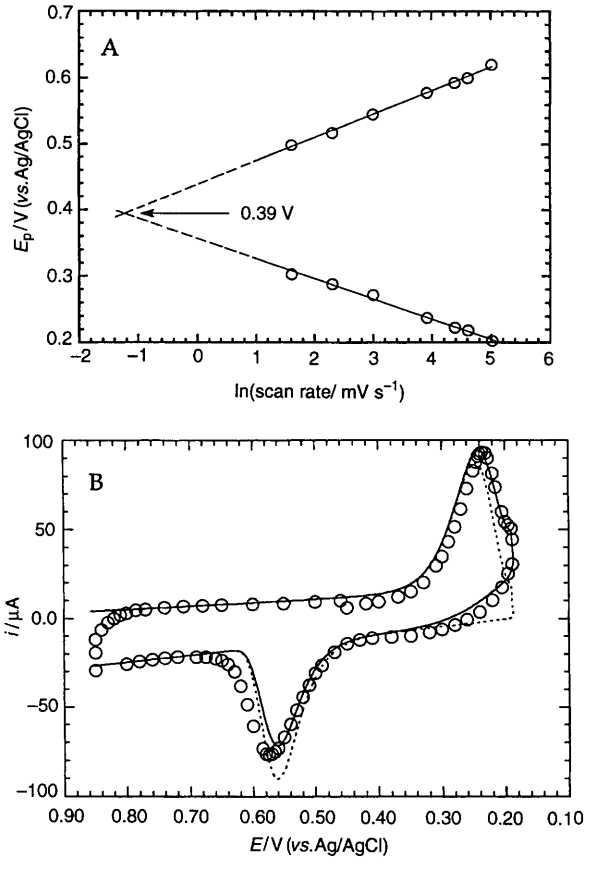

Fig. 7 A Anodic (upper line) and cathodic (lower line) peak potentials *vs.* ln(scan rate) for the reduction of O_2 at a graphite electrode on which $[(hmc)Co]^{3+}$ was adsorbed. The intersection of the extrapolated lines lead, *via* eqn. (XXV), to $E_3^f = 0.66$ V. B, Comparison of the experimental (○) and calculated (····), (——) cyclic voltammetric responses obtained with the electrode from A. Experimental parameters: $C_Z^0 = [O_2] = 1.30 \times 10^{-3}$ M, $D_Z = D_{O_2} = 1.7 \times 10^{-5}$ cm^2 s^{-1} $v = 50$ mV s^{-1}, $S = 0.32$ cm^2, $\Gamma = 1.7 \times 10^{-9}$ mol cm^{-2}. Parameters employed in the calculations of the dotted line: $E_1^f = 0.09$ V, $k_{s_1}^0 = 50$ s^{-1}, $\alpha_1 = 0.5$, $E_3^f = 0.66$ V, $k_{s_3}^0 = 50$ s^{-1}, $\alpha_3 = 0.5$, $K_2 = 2.2 \times 10^3$ M^{-1}, $k_2 = 3.5 \times 10^5$ M^{-1} s^{-1}. The solid line was obtained using the same parameters plus $E_4^f = 0.14$ V, $k_{s_4}^0 = 0.34$ s^{-1} and $\alpha_4 = 0.22$ for the reduction of $[(hmc)CoO_2H]_{ads}^{2+}$ (see text).

Conclusions

The primary purpose of this study was the application of the finite difference calculational procedure to systems that follow the ECE mechanism depicted in Scheme I. The results show that a variety of cyclic voltammetric responses can be encountered depending on the values of the kinetic parameters governing the electrode and chemical reactions. Comparison of the representative calculated responses shown in the figures with experimental responses should allow the presence of an ECE mechanism to be established in favourable cases. Procedures for estimating the relevant kinetic parameters were also described. ECE mechanisms are likely to be involved when electrocatalysts must be generated by reduction or oxidation of catalytically inactive precursors that contain redox-active metal centers. The reduction of O_2 at catalyst-coated electrodes as discussed in this report is one example of such a system. Others include the catalysis of the electroreductions of CO_2 by adsorbed Ni(cyclam)$^{2+}$ [11] and of NO by adsorbed heteropolytungstate anions,[12] respectively.

This work was supported by the U.S. National Science Foundation.

References

1 Y. Xie and F. C. Anson, *J. Electroanal. Chem.*, 1995, **384**, 145.
2 Y. Xie and F. C. Anson, *J. Electroanal. Chem.*, 1995, **396**, 441.
3 Y. Xie and F. C. Anson, *J. Electroanal. Chem.*, 1996, **404**, 209.
4 A. C. Testa and W. H. Reinmuth, *Anal. Chem.*, 1960, **32**, 1512.
5 E. Laviron and A. Vallat, *J. Electroanal. Chem.*, 1976, **74**, 297.
6 E. Laviron, in *Electroanalytical Chemistry*, ed. A. J. Bard, Marcel Dekker, New York 1982, vol. 12.
7 C. Kang, Y. Xie and F. C. Anson, *J. Electroanal. Chem.*, in the press.
8 C. P. Andrieux and J-M. Saveant, *J. Electroanal. Chem.*, 1978, **93**, 163.
9 K. Aoki, K. Tokuda and H. Matsuda, *J. Electroanal. Chem.*, 1986, **199**, 69.
10 S. W. Feldberg, in *Electroanalytical Chemistry*, ed. A. J. Bard, Marcel Dekker, New York, 1969, vol. 3.
11 M. Beley, J-P. Collins, R. Ruppert and J-P. Sauvage, *J. Am. Chem. Soc.*, 1986, **108**, 7461.
12 C. Rong and F. C. Anson, *Inorg. Chim. Acta*, 1996, **242–243**, 1.

Paper 6/01595F; *Received 6th March*, 1996